

Synthesis and Characterization of BFO Doped with Nickel

Dr Jyotsna Chauhan*, Poonam patel

*HOD Department of Nanotechnology, Rajiv Gandhi Technical University, Bhopal (M.P.), India

*Corresponding authors E-mail: jyotsnachauhan2006@gmail.com

Abstract: Motivated by the previous investigations of multiferroic material bismuth ferrite, it stimulates further efforts to synthesize perovskite solution BiFeO₃ as well as the isovalently substituted BiFeO₃, i.e. BiFe (1-x)M_xO₃ (0 ≤ x ≤ 0.2) and in order to track their phase transformations at different compositions and develop different synthesis methods that can curb the formation of impurity phases. Chemical route can be used to synthesize nanocrystalline undoped and Ni-doped bismuth ferrite with perovskite structure and crystallite size of about 14nm and 15.4 nm, respectively. Rise in doping concentration leads to generation of secondary phase, thus dopant concentration is maintained to 5 mol%. Morphological analyses exhibits irregular polygonal to bimodal shape agglomerates with few interconnected pores. Dielectric constant for the undoped bismuth ferrite is about 100, while for 5 mol% Ni doped sample it is noted around 600 (at low frequency). Such drastic change leads to higher polarizability which also enhances ferroelectricity with Ni doping on perovskite bismuth ferrite. Both nanocrystalline and Ni-doped BFO exhibits super paramagnetic nature due to suppression of spin cycloid magcycloid magnetic moment. Saturation magnetization of Ni-doped is slightly lower than for undoped BFO due to smaller crystallite size.

[Jyotsna Chauhan, Poonam patel. **Synthesis and Characterization of BFO Doped with Nickel.** *Rep Opinion* 2018;10(4):69-85]. ISSN 1553-9873 (print); ISSN 2375-7205 (online). <http://www.sciencepub.net/report>. 11. doi:[10.7537/marsroj100418.11](https://doi.org/10.7537/marsroj100418.11).

Keywords: ferroelectricity, XRD, FTIR

1. Introduction:

Nanotechnology is science, engineering, and technology conducted at the nanoscale, which is about 1 to 100 nanometers. Nanoscience and nanotechnology are the study and application of extremely small things and can be used across all the other science fields, such as chemistry, biology, physics, materials science, and engineering [1]. BFO exhibit both properties ferromagnetic as well as ferroelectric properties, meaning that it can be magnetized in the presence of electric current through the material. Applications of BFO include new magnetic memory devices, smart sensors and spintronics technologies. Integrating the BFO into the silicon substrate as a single crystal makes the BFO more efficient by limiting the amount of electric charge that “leaks” out of the BFO into the substrate. It means by controlling the leakage current we can now developed smart devices that can sense, manipulate and respond to data more quickly because it all happens on one chip – the data doesn’t need to be relayed elsewhere phase transformations at different compositions and develop different synthesis methods that can curb the formation of impurity phases. Chemical route can be used to synthesize nanocrystalline undoped and Ni-doped bismuth ferrite with perovskite structure and crystallite size of about 14nm and 15.4 nm, respectively. Rise in doping concentration leads to generation of secondary phase, thus dopant concentration is maintained to 5mol%. Morphological analyses exhibits irregular polygonal to

bimodal shape agglomerates with few interconnected pores. Dielectric constant for the undoped bismuth ferrite is about 100, while for 5mol% Ni doped sample it is noted around 600 (at low frequency). Such drastic change leads to higher polarizability which also enhances ferroelectricity with Ni doping on perovskite bismuth ferrite. Both nanocrystalline and Ni-doped BFO exhibits super paramagnetic nature due to suppression of spin cycloid magcycloid magnetic moment. Saturation magnetization of Ni-doped is slightly lower than for undoped BFO due to smaller crystallite size.

1.1 Multiferroics

The simultaneous coexistence of at least two ferroic properties, (anti) ferromagnetism, (anti) ferroelectricity and (anti) ferroelasticity in the same phase is defined as multiferroics, as shown in Figure 1.2. These materials have the potential of exhibiting coupling between and magnetism, known as the magnetoelectric effect, which enables the external electric field to change magnetization and vice versa.

However, looking back in history, the combination and correlation of magnetism and electricity were well interpreted by Maxwell equations in the 19th century, but magnetic and electric ordering in solids were always treated separately at that time. This is because the magnetic properties were understood to be attributed to the spin of electrons while the electric properties the electric charges of ions and electrons.

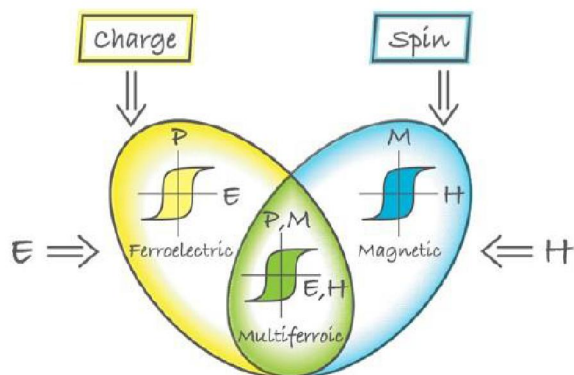


Figure 1.2 Schematic illustration of multiferroic defined from the overlap region of ferroelectric and magnetic

This can be partly improved by introducing dopants (such as rare-earth elements) into the original material. Moreover, since the microscopic origin of magnetism can be described as the presence of localized electrons, mainly in the partially filled d or f shell of transition metals or rare-earth ions having a corresponding localized spin. By contrast, ferroelectric materials require transition metal ion with an empty d shell, and the displacement of such transition metal ion towards an apical atom (normally oxygen) creates electric dipoles that are stabilized by the strong covalent bonds between O 2p and empty d orbitals. The mutual exclusion of ferroelectricity and magnetism give rise to a problem called "d⁰versus dn". In order for the coexistence of magnetism and ferroelectricity to occur, both the elements and structures need to be considered. In the perovskite type structure (ABO₃) multiferroics, the A site element is selected to take the responsibility for the ferroelectricity while the element at the B site accounts for the magnetism. For instance in the perovskite BiMnO₃, the 6s² lone pair of Bi³⁺ tends to hybridize with O 2p orbital, which improves the ferroelectricity by driving the Bi³⁺ towards the oxygen ions, while the Mn cation has non-zero d-electrons bonds between O 2p and empty d orbitals. The mutual exclusion of ferroelectricity and magnetism give rise to a problem called "d⁰versus dn". In order for the coexistence of magnetism and ferroelectricity to occur, both the elements and structures need to be considered. In the perovskite type structure (ABO₃) multiferroics, the A site element is selected to take the responsibility for the ferroelectricity while the element at the B site accounts for the magnetism. For instance in the perovskite BiMnO₃, the 6s² lone pair of Bi³⁺ tends to hybridize with O 2p orbital, which improves the ferroelectricity by driving the Bi³⁺ towards the oxygen ions, while the Mn cation has non-zero d-electrons [8].

The potential application of multiferroics is quite extensive and promising, ranging from giant electric transformers to a small computer memory devices or even tiny sensors. Unfortunately, most of the multiferroics are not naturally-occurring materials and fewer materials possess magneto electric properties. Majority of multiferroic materials have low magnetic ordering and ferroelectric transition temperature. This can be partly improved by introducing dopants (such as rare-earth elements) into the original material. Moreover, since the microscopic origin of magnetism can be described as the presence of localized electrons, mainly in the partially filled d or f shell of transition

metals or rare-earth ions having a corresponding localized spin. By contrast, ferroelectric materials require transition metal ion with an empty d shell, and the displacement of such transition metal ion towards an apical atom (normally oxygen) creates electric dipoles that are stabilized by the strong covalent bonds between O 2p and empty d orbitals. The mutual exclusion of ferroelectricity and magnetism give rise to a problem called "d⁰versus dn". In order for the coexistence of magnetism and ferroelectricity to occur, both the elements and structures need to be considered. In the perovskite type structure (ABO₃) multiferroics, the A site element is selected to take the responsibility for the ferroelectricity while the element at the B site accounts for the magnetism. For instance in the perovskite BiMnO₃, the 6s² lone pair of Bi³⁺ tends to hybridize with O 2p orbital, which improves the ferroelectricity by driving the Bi³⁺ towards the oxygen ions, while the Mn cation has non-zero d-electrons bonds between O 2p and empty d orbitals. The mutual exclusion of ferroelectricity and magnetism give rise to a problem called "d⁰versus dn". In order for the coexistence of magnetism and ferroelectricity to occur, both the elements and structures need to be considered. In the perovskite type structure (ABO₃) multiferroics, the A site element is selected to take the responsibility for the ferroelectricity while the element at the B site accounts for the magnetism. For instance in the perovskite BiMnO₃, the 6s² lone pair of Bi³⁺ tends to hybridize with O 2p orbital, which improves the ferroelectricity by driving the Bi³⁺ towards the oxygen ions, while the Mn cation has non-zero d-electrons [8].

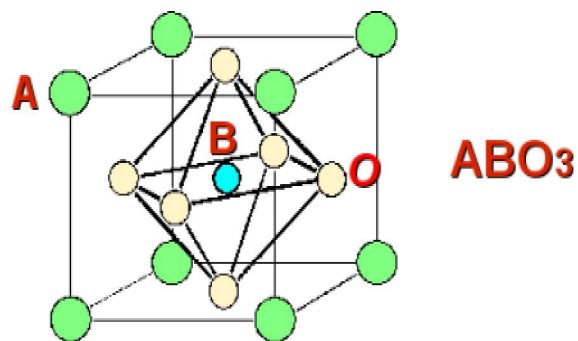


Figure 1.2

In fact, perovskite can be viewed from different perspectives. The stereo picture presented above is a B-cell setting with B-site at the origin and A-site in the center of eight octahedra. However, A-cell setting is also exist and preferred in some cases, where perovskite is originated from A-site and making B-site positioned at the center of the cell (Figure 1.3).

Figure 1.3 Perovskite structure of A-cell setting with B-site positioned at the center of the unit cell. For materials with perovskite structures, it can be an ideal structure without any tilting and distortions. [9]

However, under certain conditions, structures with ion displacement or/and octahedral tilting might take place, which could change their original symmetry and unit cell parameters.

1.2 Introduction Of Bismuth Ferrite:

Bismuth ferrite (BiFeO_3), is an inorganic chemical compound with a perovskite structure and an unusual compound of bismuth, iron, and oxygen (BFO). It is one of the most promising lead-free piezoelectric materials, which exhibits multiferroic properties at room temperature. Multiferroic materials exhibit ferroelectric or anti-ferroelectric properties in combination with ferromagnetic (or antiferromagnetic) properties in the same phase. As a result, an electric field can induce change in magnetization and an external magnetic field can induce electric polarization. This phenomenon is known as the magneto electric effect (ME) effect and materials exhibiting this effect are called magneto electrics or seignetto-magnets. Further proof of it being ferromagnetic is that it produces a hysteresis loop during ferroelectric characterization. The ability to couple to either the electric or the magnetic polarisation allows an additional degree of freedom in device designs. [10]

However one of the major drawbacks of the material is its high current leakage. Therefore it allows current to pass through when a high voltage is applied. Attempts to improve the electrical properties have been made by doping it with rare earth elements such as lanthanum (La), samarium (Sm), gadolinium (Gd),

terbium (Tb) and dysprosium (Dy) etc. The dopant can be at the A site or the B site. A site being the edges of the perovskite cell and the B site being the centre of the perovskite cell. The local short-range magnetic ordering of BiFeO_3 is G-type anti-ferromagnet, that is, each Fe_2O_3 spin is surrounded by six anti parallel spins on the nearest Fe neighbors. [11]

Bismuth ferrite (BiFeO_3 abbreviated as BFO), which is known to be the only multiferroic compound that exhibits simultaneous ferroelectric and G-type anti ferromagnetic orders over a broad range above room temperature (Curie temperature $>800^\circ\text{C}$, Neel temperature = 370°C) As a partially covalent oxide, BFO has a rhombohedrally distorted perovskite structure belonging to a space group of $R3c$ [7]. Nevertheless, it exhibits weak magnetism at room temperature due to a spiral magnetic spin cycloid with a periodicity of $\sim 62\text{nm}$ [4]. So far, most studies on BFO have been performed on two-dimensional epitaxial thin films grown on various substrates [8–11], where epitaxial strain is manifested so as to alter some important properties including crystal lattice structure, polarization, and magnetization. However, more recent approaches are focusing on polycrystals as well as substrate-free nanostructures such as low-dimensional nanostructures, especially zero-dimensional materials like nanoparticles (NPs). Several chemical routes (e.g. hydrothermal treatment, mechanochemical synthesis method, and sol-gel methodology, etc.) have been successfully employed for fabricating BFO nanoparticles. But in our lab this product is synthesized by solgel method, at low temperature approx. at 200°C .

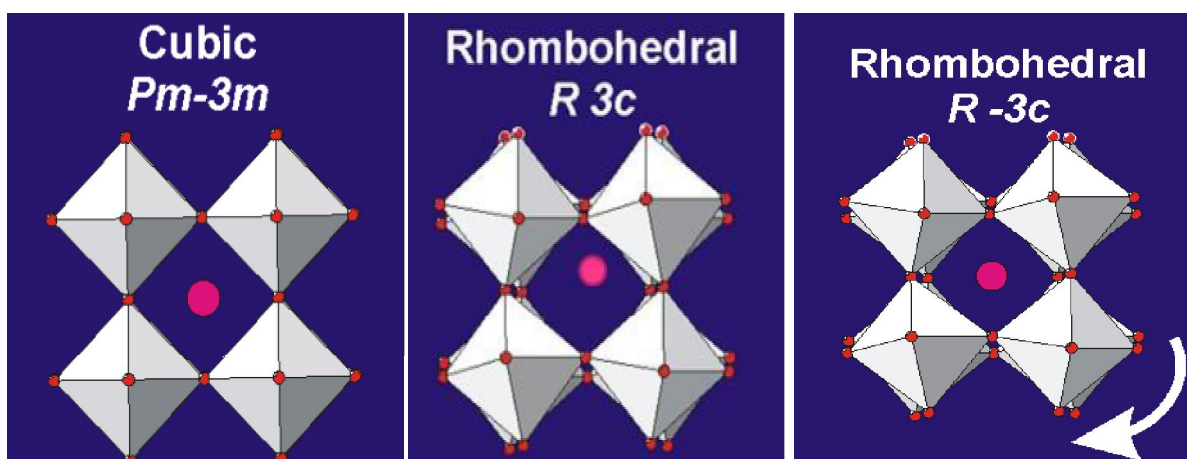


Figure 1.7 Schematic illustration of a structural transition process (a) ideal cubic structure $Pm-3m$ without tilting ($a_0a_0a_0$); (b) $R-3c$ structure tilted along three axes with the same angle ($a-a-a$); (c) Displacement of Bi ion towards $[111]$ direction based on $R-3c$.

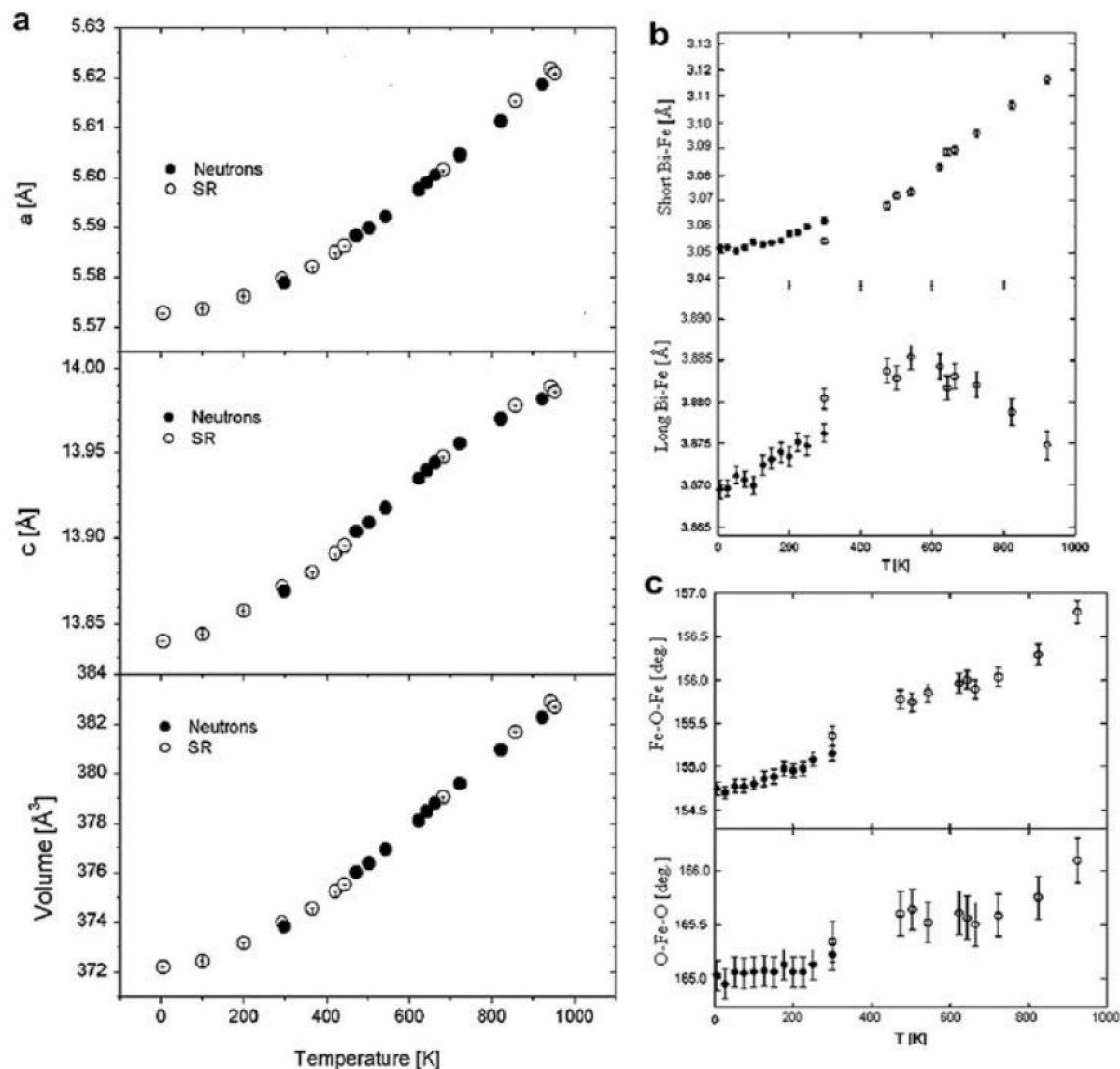


Figure 1.8 Plots of temperature (0-1000K) as functions of (a) lattice parameter *a*, *c* and volume of BiFeO₃ (b) short and long distance of Bi-Fe bond (c) Fe-O-Fe and O-Fe-O angles. [18]

BFO NPs through solutions of some specific salts at a temperature of 600°C [23]. Despite the efforts made through enhancing sintering temperature to avoid impurities, a small amount of Bi₂O₃ was found in the final product [24]. The resulting size of BFO NPs was sometimes large (up to several hundred nanometers) although no impurities were found in the final products. Using the same method, prepared pure phase BFO nano crystallites at 200°C using KOH concentration of 4M. In this study, impurity phases of Bi₂Fe₄O₉ and Bi₂₅Fe₄O₄₀ were easily formed with only a slight change in the KOH concentration [5]. Although pure phase BFO was obtained in this study, contaminant produced by decomposition of the precursor was present. Synthesized nano sized bismuth ferrite using a soft chemical route with tartaric acid as a template material and nitric acid as an oxidizing

agent [7]. However, the crystallinity of the resulting BFO NPs was unsatisfactory and the existence of an impure Bi₂O₃ amorphous phase in the host at low temperature product of 400°C was evident.

To deal with the issues mentioned above, our recent research suggests that excess tartaric acid and/or citric acid to be added in the solution so that the crystallinity of BFO NPs can be improved. Here in, we reported a general sol gel route for synthesizing uniform BFO NPs at about 350°C. To our best knowledge, this is the lowest temperature employed in the literature for BFO fabrication with the exception of certain high pressure techniques such as hydrothermal or solvo thermal methods. In addition, the magnetic properties were also investigated for BFO NPs with different size and hence known as “promising” material for the fabrication of visible light emitting

devices distributions. Bismuth ferrite (BiFeO_3) is one of the few multiferroics that has Curie and Neel temperatures above room temperature. magnetoelectric coupling is realized at room temperature and such coupling is strongly enhanced by proper dopings. It has also been reported that the low symmetry monoclinic or tetragonal thin film BiFeO_3 might be the origins of strong polarization. [12, 13] Until recently, increasing efforts have also been devoted to the research focusing on the preparation and characterization of BiFeO_3 in forms of bulk and nanostructure. [14, 15]. Single phase BiFeO_3 has rhombohedrally distorted perovskite structure $R3c$ with antiphase rotation of FeO_6 octahedra by 12° , denoted as a-a-a-in the Glazer notation. The displacement of the A-site bismuth cation along the $[111]$ pseudo-cubic axis brings about a non-centrosymmetric polarization resulting in the ferroelectric property. The actual structure of BiFeO_3 can be understood by an imaginary structural transition process, as shown in Figure 1.7. The lattice parameters for bismuth ferrite with rhombohedral structure are 3.965\AA and $89.4^\circ 16'$ or $a=5.58\text{\AA}$ and $c=13.9\text{\AA}$ if viewed in the hexagonal setting at room temperature. [15]

The lattice parameter and crystal structure of BiFeO_3 are dependent on the temperature. The atomic

coordination are slight changed between 5K and 300K. Significant changes are observed above 300K, the influence of temperature on the cell parameter, volume, bond distance and bond angle are shown below in Figure 1.8.

It was well documented that, except for the long Bi-Fe bond distance, the lattice parameter a , c , the volume of unit cell, the short bond distance of Bi-Fe as well as the bond angles gradually increase with increase in temperature. As a consequence of these variations, magnetism and polarization are reported to be gradually reduced, and structural phase transitions are also induced from the rhombohedrally distorted $R3c$ perovskite structure to an orthorhombic $Pnma$ structure at 1098K and eventually to a cubic structure above 1204K. [19]

However, single phase BiFeO_3 is difficult to synthesize. Due to the metastable nature of bismuth ferrite in air [20] as well as the volatility of bismuth oxide, their stoichiometry can be changed resulting in impurities of Bi_2O_3 , $\text{Bi}_{25}\text{FeO}_{39}$ and Bi_2FeO_9 during the sintering process. The phase diagram of Fe_2O_3 and Bi_2O_3 is presented below in Figure 1.9 [20], unequal amount of Fe_2O_3 and Bi_2O_3 is seen to bring about impurity phases $\text{Bi}_{25}\text{FeO}_{39}$ (bismuth-rich) and Bi_2FeO_9 (bismuth-deficient).

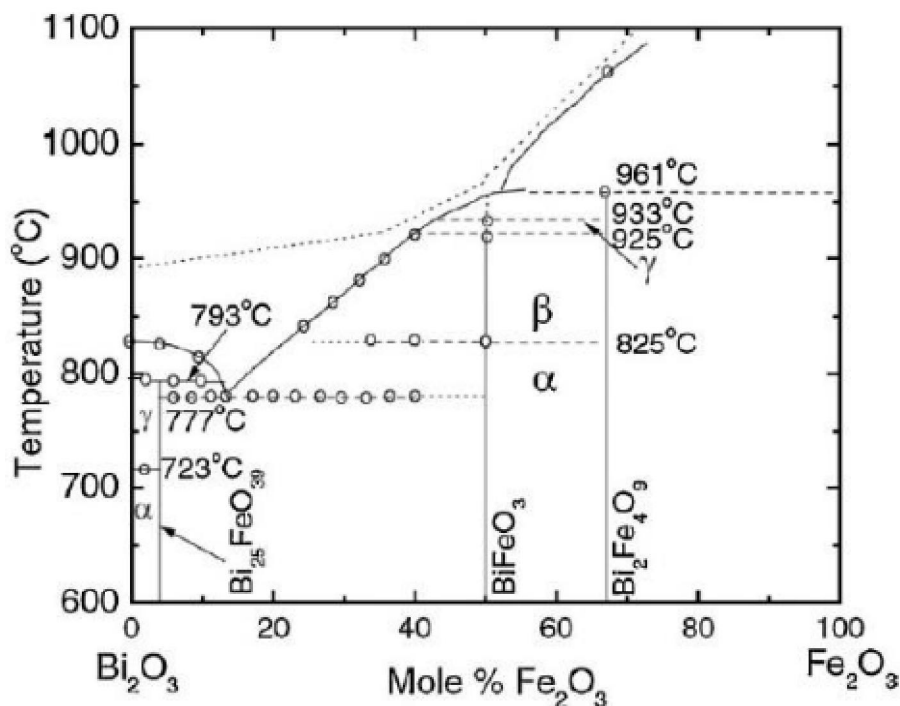


Figure 1.9 Phase diagram of Fe_2O_3 and Bi_2O_3 showing bismuth ferrite with undesired impurities. [12]

2. Experimental: Many techniques have been utilized to prepare BiFeO_3 nanostructures. All of the reagents were of LR grade and used without further

purification. Following a typical procedure, of bismuth nitrate [$\text{Bi}(\text{NO}_3)_3 \cdot 5\text{H}_2\text{O}$] and iron nitrate [$\text{Fe}(\text{NO}_3)_3 \cdot 9\text{H}_2\text{O}$] were weighed in stoichiometric

proportions and dissolved in deionized water to make a solution with an independent concentration of 0.1M before adding 20mL diluted nitric acid (65~68% HNO_3) to the mixture. The light-yellow-colored solution was heated under vigorous stirring until no liquid was left in the beaker to form gel deposit. Each beaker with solid deposit was kept in the oven at 150°C for another 2-3h. Subsequently, powders were quarterly divided and calcined in the

oven for 10-12 h at 550°C, respectively, to obtain well-crystallized BFO NPs with controllable sizes.

For comparison, another group of powders were synthesized by modifying a typical soft chemical route by using excess tartaric acid as chelating agents [27].

The gel (intermediate product) was subjected to thermal analysis in order to determine the subsequent sintering temperature with simultaneous Mofel furnace. After heat treatment, the sample was characterized using X-ray diffraction. Fourier transformation infrared (FT-IR) spectra were obtained.

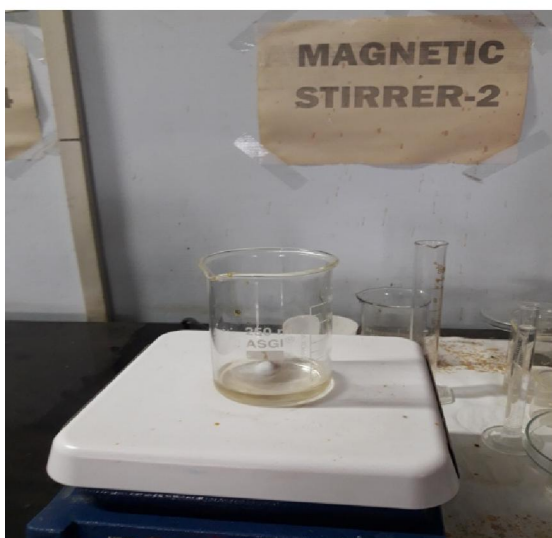
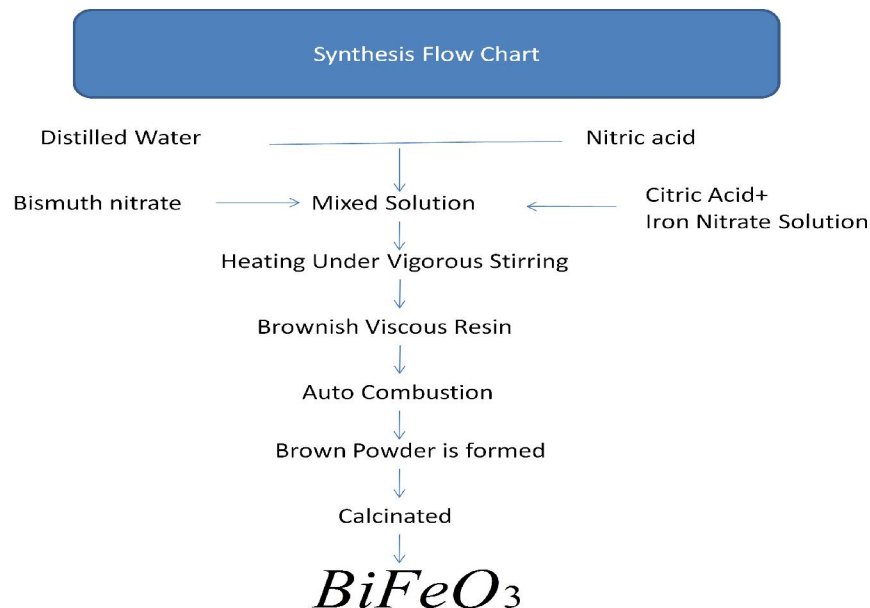


Figure 2.5 Diagram of pure BFO during stirring

Figure 2.5 is the picture of sample when we add the bimuth nitrate in the solution of DI water and nitric acid after this the sample is stirred being the colour of the should be transparent it means the process of

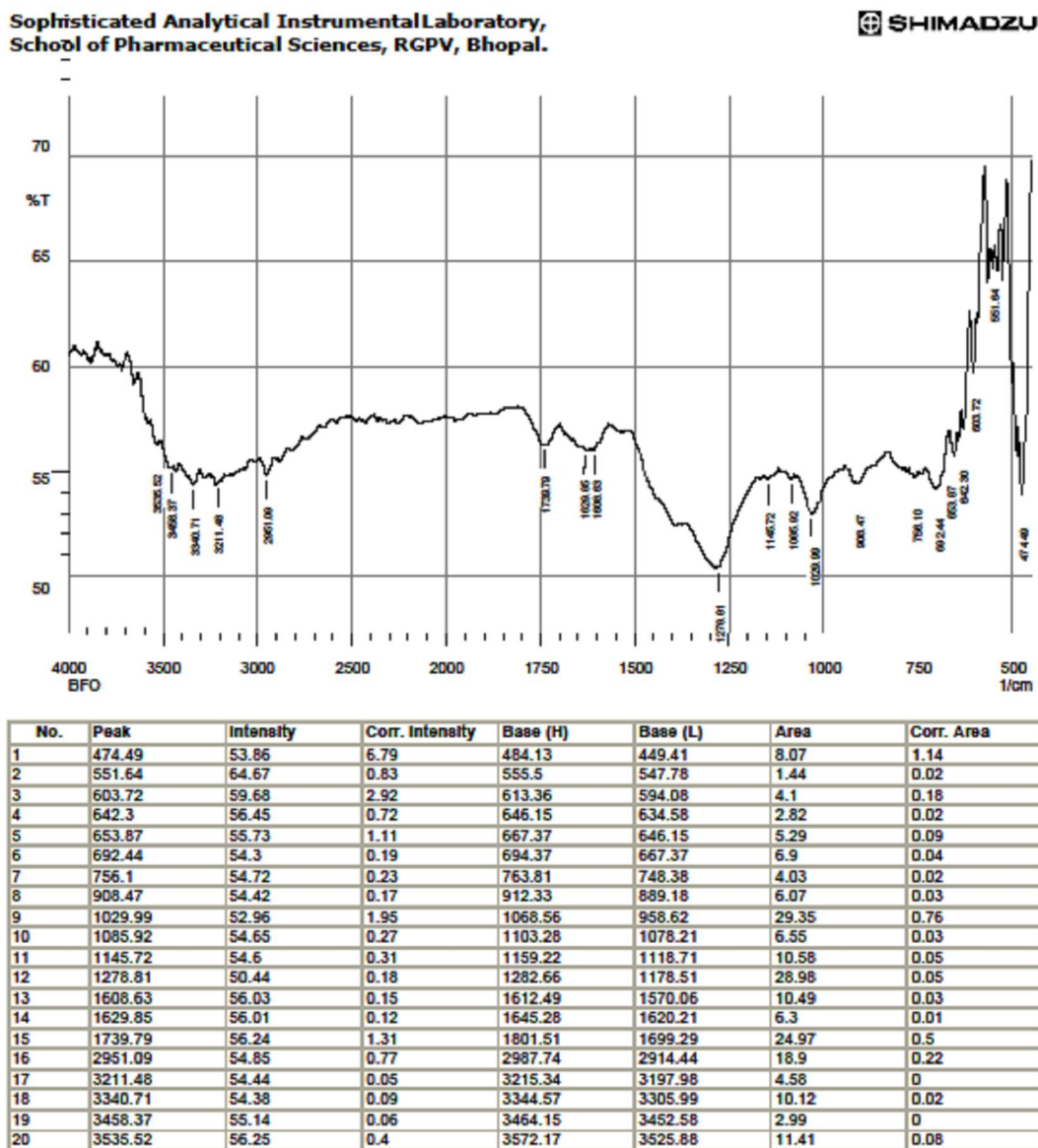
If the colour of the



Figure 2.6 Diagram of pure BFO during stirring after adding citric acid

Figure 2.6 is the picture of sample when we add both the solution with each other means colour of the sample is light yellow but after adding citric acid to the solution the colour of the sample is brown in

colour this sample is stirred 12 to 15 hr for homogeneous solution after this sample is heated at 150°C for 3-4 hr to calcinated the sample.



Comment; BFO

Date/Time; 6/23/2017 2:57:27 PM No. of Scans; Resolution;

User; Administrator

Figure 2.7 FTIR Diagram of pure BFO

PXRD:

X-rays are a type of electromagnetic radiation. The wavelength of x-rays is approximately 1 Å which has the same size equivalent to that of an atom. Powder X-ray diffraction (PXRD) is a non-destructive analytical technique mainly used for the phase identification and structural characterization of

crystalline materials. Powder X-ray diffraction combined with Rietveld analysis, provides detailed information regarding unit cell dimensions, bond-lengths, bond-angles and the site ordering of crystallites. The relationship between the wavelengths of the X-rays λ , the incidence angle 2θ and spacing

between two crystal lattice planes (hkl) d , is shown in the Bragg's Law expressed as: $n\lambda=2d\sin\theta$.

After characterization by Powder X-ray diffraction, a number of peaks are seen in the diffraction patterns. These peaks are identified by comparing their positions and relative intensities with the known structures in the database (such as database developed by the IISER for Diffraction Data). Sometimes extra peaks might appear due to the impurity or structural transformation after thermal treatment. In fact, the intensities, widths and positions of peaks in the patterns reflect information about structure, quantity, texture etc. of crystallites. Almost all the factors are linked to certain parameters that can be refined by computer programs in our computer we refined the XRD by using origin software. [18]

Thermal Analysis

Detail information regarding mass changes and caloric effects of a sample during heating and cooling process can be measured simultaneously. A plot of

mass change and heat flow as a function of temperature can be obtained in one graph upon heating and cooling.

There is a highly sensitive balance with two identical crucibles placed on both sides, one of which serves as a reference that should keep always empty and clean. Before performing the thermal analysis, the instrument is supposed to be calibrated by making two empty crucibles balanced first. After filling one of the crucibles with the test sample, a gradual heating process is introduced inside the chamber with gas flow at certain speed. Before getting an reliable experimental result, a baseline correction is required by subtracting the empty crucible run from the original sample run.

The purpose of using this thermal analysis is to specify the water of hydration in the reagents of nitrates for the solution synthesis and to determine the antiferromagnetic ordering temperature T_N and ferroelectric temperature T_c .

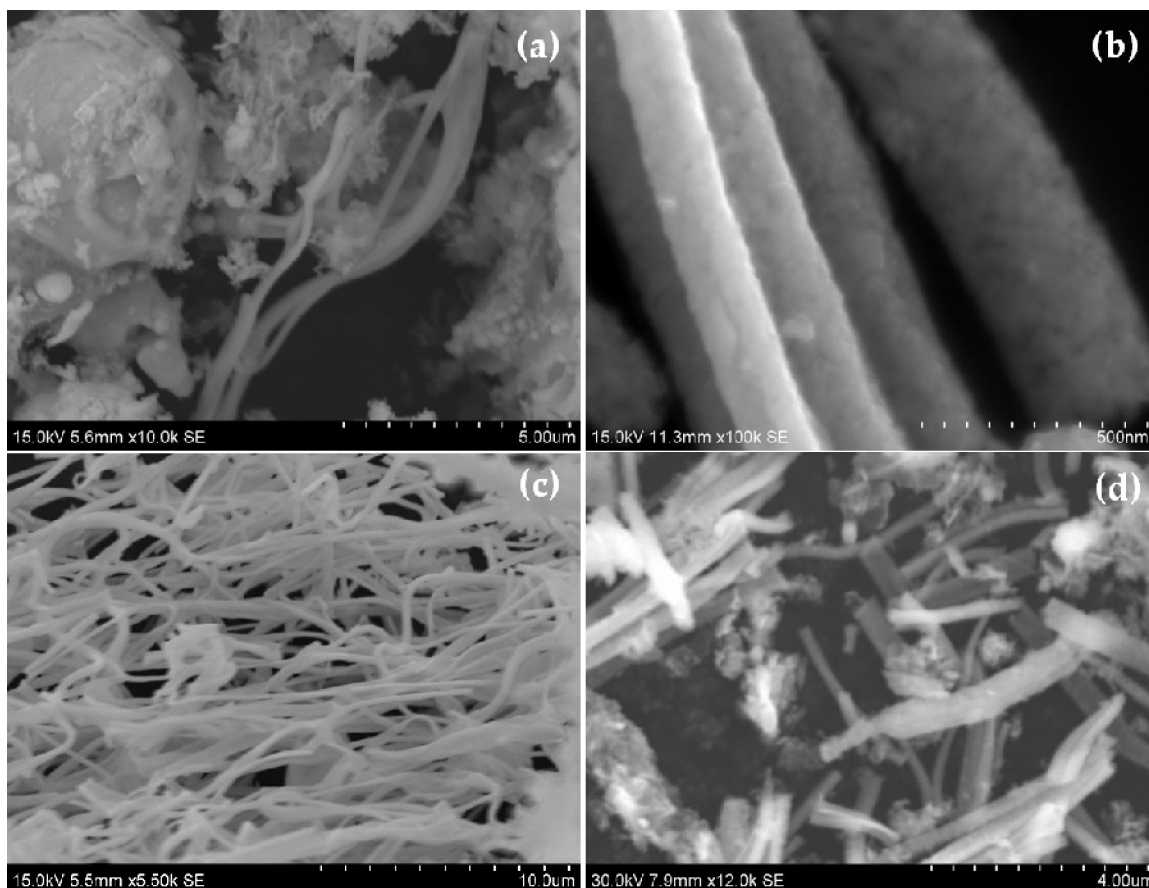


Figure 2.8 SEM Diagram of Pure BFO

- (a) 8 kv it 's not sufficient Small diameter.
- (b) 10 kv large diameter, Poor mechanical strength.
- (c) 15 kv excellent fiber, homogenous Size distribution, diameter of size 50-100 nm
- (d) 20 kv very small length, were fibers are broken relatively in homogenous.

Ftir Result:

FTIR, is used to measure a sample by absorbs light at each wavelength. FTIR measure how much of the light is absorbed, and repeat for each different wavelength.

Fourier transform spectroscopy technique shines a beam containing many frequencies of light at once, and measures how much of that beam is absorbed by the sample. Next, the beam is modified to contain a different combination of frequencies, giving a second data point. This process is repeated many times. Afterward, a computer takes all this data and works backward to infer what the absorption is at each wavelength.

The beam described above is generated by starting with a broadband light source—one containing the full spectrum of wavelengths to be

measured. The light shines into a Michelson interferometer—a certain configuration of mirrors, one of which is moved by a motor. As this mirror moves, each wavelength of light in the beam is periodically blocked, transmitted, blocked, transmitted, by the interferometer, due to wave interference. Different wavelengths are modulated at different rates so that at each moment the beam coming out of the interferometer has a different spectrum.

As mentioned, computer processing is required to turn the raw data (light absorption for each mirror position) into the desired result (light absorption for each wavelength). The processing required turns out to be a common algorithm called the Fourier transform (hence the name, "Fourier transform spectroscopy").

2.14 X-Ray diffraction result:

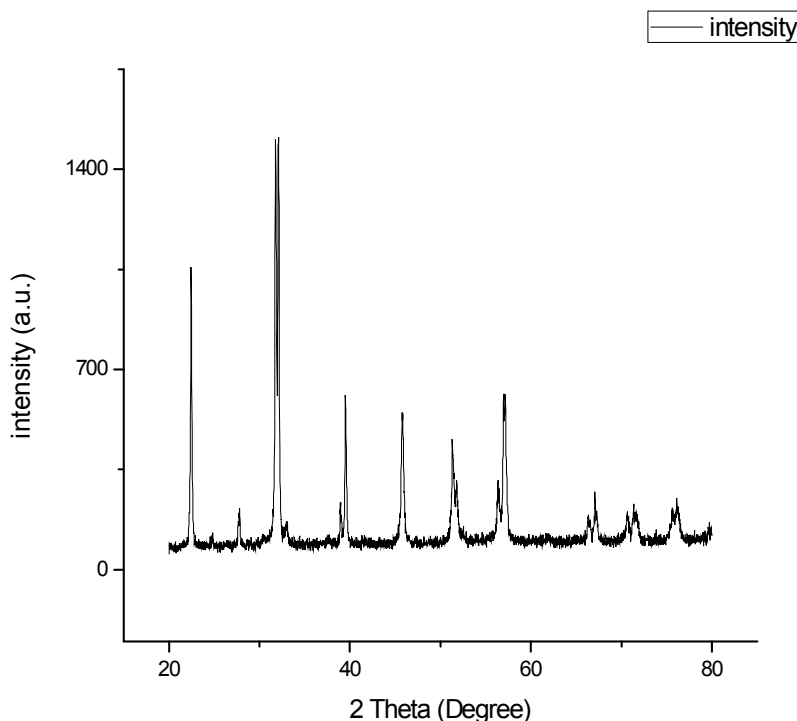


Figure 2.9 Powder x-ray diffractogram for BFO

Calculation of Particle size:

$$\text{Particle size} = 0.89\lambda / \beta \cos \theta$$

Here $\lambda = 1.54 \text{ \AA}$, $\beta = \text{FWHM}$,

$$\text{Then particle size} = 0.9 * 1.54 \text{ \AA} / \beta * 0.0174 * \cos \theta,$$

So

$$\text{FWHM} = x_2 - x_1, > 33 - 32 = 1 \text{ \AA}^\circ, \text{ FWHM} = 0.1 \text{ nm},$$

then and $2\theta = 31.6059$, $\theta = 15.80$, then $\cos \theta = 0.9622$

$$\text{And Particle size} = (0.89 * 1.54) / (1 * 0.962) = 14.24 \text{ nm}.$$

INTERPLANAR SPACING

$$n\lambda = 2d \sin \theta \quad n=1, 2, \dots, \text{ Here } n=1$$

Sin (11.245)	d=4.05 \AA
Sin (13.968)	d=3.19 \AA
Sin (15.8807)	d=2.8143 \AA
Sin (19.7053)	d=2.28 \AA
Sin (23.0098)	d=1.97 \AA
Sin (25.8007)	d=1.77 \AA
Sin (28.6694)	d=1.605 \AA
Sin (33.5952)	d=1.39 \AA

Table 2.1

XRD measurements were performed to characterize the crystal structure of the calcined

powders. As shown in Figure 2.5, all the XRD patterns can be indexed to pure rhombohedral perovskite structure, which are in good agreement with the powder of pure BFO sample.

After heat treatment at 350°C, the sample from nitric acid precursor begins to generate pure phase BFO while another sample from sodium hydroxide acid precursor is still of amorphous feature. It is clear that the crystallization of BFO completed at a temperature of 350°C for nitric acid precursor while 450°C for sodium hydroxide acid precursor, which is used to reduce the effect of nitric acid. Meanwhile, the particle size of BFO changed remarkably after further heat treatment.

Calcined at temperatures above 550°C, well-crystallized and pure phase BFO can be obtained for either precursor. As discussed in early literatures, the grain sizes of BFO NPs grow up with increasing the temperature in soft chemical routes [21, 26]. This can be also confirmed by the peak sharpening of XRD curves.

2.15 Experimental results on BiFeO₃ and related compound

Multiferroic materials exhibit electric and magnetic natures which result in a mutual existence of ferroelectricity and ferromagnetism in a single phase [1]. Because of room-temperature coupling between ferroelectric and magnetic order parameters, it brings forth a novel phenomenon known as magnetoelectric effect (ME), in which polarization can be tuned by magnetic field and vice versa. This coupling provides an additional opportunity for the design of magnetoelectric and spintronic devices [2–4]. Multiferroic materials have gained tremendous attention on account of their potential applications in various fields, such as bubble memory device, microwave, satellite communication, audio-video, digital recording [4,5], sensor, multiple state memory element, electro-ferromagnetic resonance. device [6], thin film capacitor, non-volatile memory [7], optoelectronics, solar energy device [4], high density ferroelectric magnetic random access memory [8], and permanent magnet [9]. A multifunctional BiFeO₃ compound demonstrates a magnetoelectric coupling having Curie temperature $T_C \approx 1100$ K and G-type antiferromagnetism temperature $T_N \approx 640$ K [10,11].

However, BiFeO₃ has serious problems as a ferroelectric material because of its quite large leakage current density at room temperature, which is mainly attributed to the oxygen vacancy and oxidation state of Fe. Therefore, the higher conductive nature of BiFeO₃ makes it hard to get excellent ferroelectric property. To overcome this problem, various approaches have been proposed, such as reduction in oxygen vacancies, domination of the ohmic conduction, and intergrain depletion in grain boundary limited conduction. The

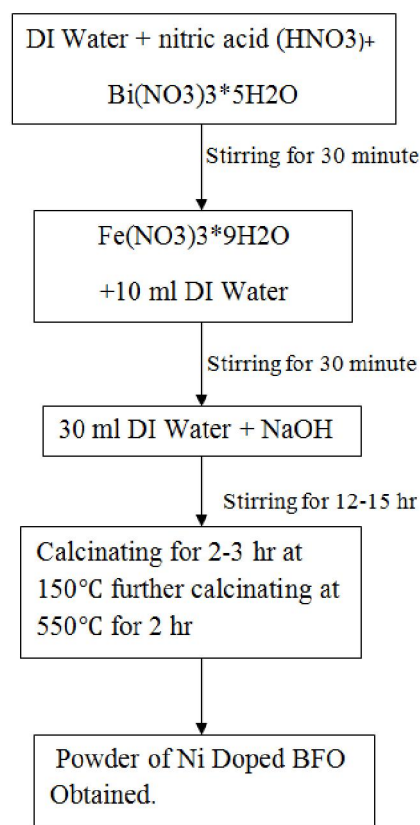
efforts have been made to reduce the leakage current density by either introducing dopants or using different fabrication methods [12–16]. At present, many researchers are engaged in the enrichment of multiferroic properties of BiFeO₃-relevant materials, using different trivalent dopants such as La [17], Mn [18], Sm [19] and Ti [20]. There are many reports on the ferroelectric and magnetic behaviors of BiFeO₃. Xu.

et al. [21] observed a room-temperature saturated magnetic hysteresis loop in Zn-doped BiFeO₃ ceramic by rapid sintering method. Chaudhari *et al.* [3] observed a superparamagnetic nature at 5 K and weak ferromagnetic behavior in BiFe_{1-x}Zn_xO₃ ($0.05 \leq x \leq 0.15$) ceramic by solution combustion method (SCM).

The multiferroic Bi_{1-x}Ca_xFeO₃ ceramic presents enhanced magnetic property which suppresses spin modulated structure [22]. Recently, Wang *et al.* [23] reported the enhanced magnetic property of Ni-substituted BiFeO₃ at doping concentration of 0.5% by hydrothermal method.

Amid this vision, the present paper investigates the structural, magnetic and dielectric properties of BiFeO₃ doped by Ni at Fe site.

2.16 Flow Chart Of Synthesis Routes For Nickel Doped BFO



2.17 Experimental effect of Nickel Doped BFO:



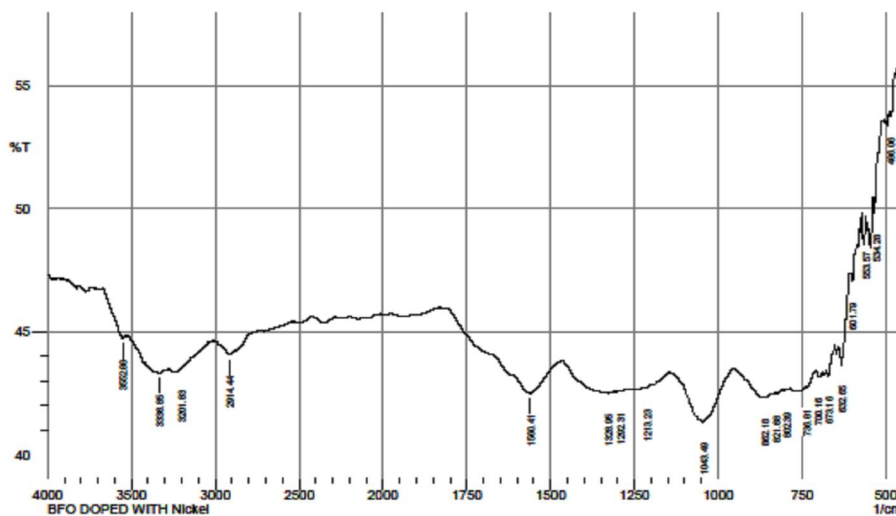
Figure 2.8 picture of Ni Doped sample at various condition

BFO and Ni-doped BFO of $\text{BiFe}_{1-x}\text{Ni}_x\text{O}_3$ were prepared by chemical route using precursor materials like bismuth nitrate $[\text{Bi}(\text{NO}_3)_3 \cdot 5\text{H}_2\text{O}]$, ferric nitrate $[\text{Fe}(\text{NO}_3)_3 \cdot 9\text{H}_2\text{O}]$, nickel nitrate and nitric acid. The solution was made of bismuth nitrate and ferric nitrate in 1:1 stoichiometric molar ratio, dissolved in the nitric acid and DI water. Each precursor was dissolved in the respective solvent to form a solution under constant stirring for 30 minutes. After ensuring that there is no sedimentation/precipitation, both precursors were mixed together and kept constant stirring for 12-15hr to homogenize mixing. The solution was subsequently heated to 150°C for drying till (2–2.5 h) all liquids gets evaporated. The calcined sample was then quickly raised to proper thermal treatment temperatures of 550°C for 10–12 hour. The samples were leached using NaOH (20–30 drops) to remove impure phases and to balance the effect of nitric acid and obtain the phase pure undoped BFO and nickel doped BFO material.

The pelletized samples were then sintered at the same conditions used for heat treatment of the as-synthesized powder samples.

2.18 Characterization Techniques Used In Nickel Doped BFO:

Sophisticated Analytical Instrumental Laboratory,
School of Pharmaceutical Sciences, RGPV, Bhopal.



No.	Peak	Intensity	Corr. Intensity	Base (H)	Base (L)	Area	Corr. Area
1	486.06	53.76	0.56	489.92	474.49	4.1	0.06
2	534.28	49.81	0.81	536.21	511.14	7.09	0.02
3	553.57	49.09	0.21	559.36	551.64	2.37	0.01
4	601.79	47.06	0.44	603.72	586.36	5.57	0.02
5	632.65	43.66	1.1	636.51	609.51	9.3	0.18
6	673.16	43.2	0.38	677.01	653.87	8.31	0.05
7	700.16	43.14	0.22	709.8	690.52	7.02	0.02
8	736.81	42.72	0.09	738.74	711.73	9.89	0.02
9	802.39	42.61	0.05	808.17	786.96	7.85	0.01
10	821.68	42.46	0.1	829.39	810.1	7.16	0.01
11	862.18	42.32	0.05	867.97	844.82	8.63	0.01
12	1043.49	41.34	2.09	1143.79	954.76	70.47	1.99
13	1213.23	42.72	0.02	1215.15	1145.72	25.45	0.03
14	1292.31	42.58	0.01	1294.24	1271.09	8.57	0
15	1328.95	42.5	0.02	1332.81	1307.74	9.31	0
16	1560.41	42.49	0.98	1614.42	1477.47	50.19	0.72
17	2914.44	44.06	0.27	2974.23	2881.65	32.79	0.12
18	3201.83	43.47	0.04	3205.69	3159.4	16.67	0
19	3336.85	43.31	0.07	3346.5	3311.78	12.6	0.02
20	3552.88	44.75	0.1	3570.24	3543.23	9.41	0.01

Comment:

BFO DOPED WITH
Nickel

Figure 2.9 FTIR Diagram of BFO Doped with Nickel

The above figure gives the information of compression and expansion of particle after doping of Nickel in BFO, with the help by establish the relationship between frequency and wave number.

Shows the room temperature UV-visible diffuse reflectance spectra of Bi_{1-x}Ni_xFeO₃ samples. It seems that pristine BFO nano particles exhibit two absorption peaks at 475nm and 585nm, which shift to a lower wavelength in case of doped samples. As a semiconductor, it is well-known that the optical absorption properties of BFO are related to the

electronic structure and play the key role in determining their bandgaps. The energy bandgaps (E_g) of samples were calculated by classical Tauc formula. In this case, the absorption coefficient α (here $\alpha^{1/4} \propto \pi k/\lambda$) and the photon energy $h\nu$ for directly allowed transitions are related as: $(\alpha h\nu)^2 \propto A (h\nu - E_g)$, where A is a constant function. The E_g values are therefore determined by extra polating the linear portion of the plot relating $(\alpha h\nu)^2$ versus $h\nu$ to $(\alpha h\nu)^2 \propto 0$.

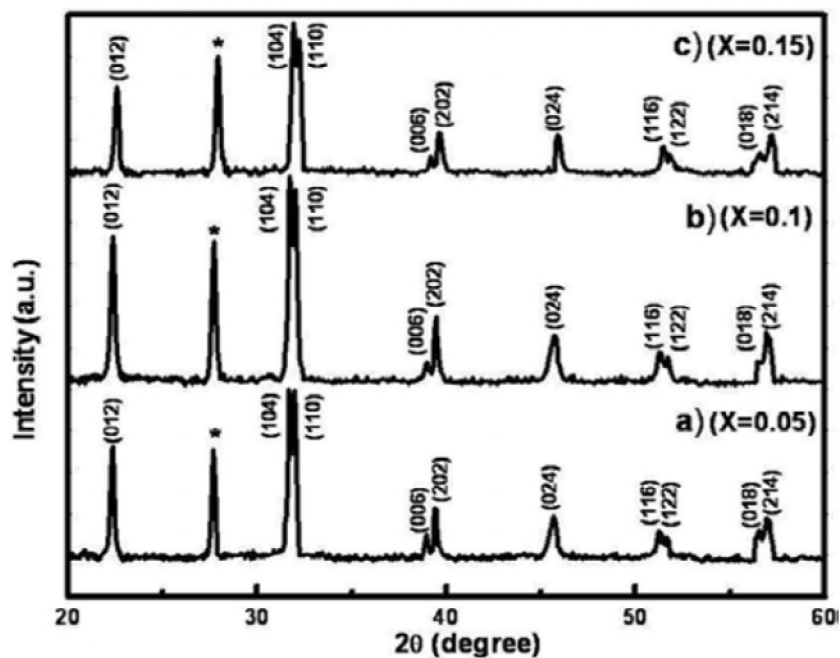


Figure 2.10 XRD Diagram of BFO Doped with Nickel

Figure 2.11 demonstrates the room-temperature X-ray diffraction (XRD) patterns of $\text{BiFe}_{0.95}\text{Ni}_{0.05}\text{O}_3$, $\text{BiFe}_{0.9}\text{Ni}_{0.1}\text{O}_3$ and $\text{BiFe}_{0.85}\text{Ni}_{0.15}\text{O}_3$ ceramics. The XRD

patterns depict that, $\text{BiFe}_{1-x}\text{Ni}_x\text{O}_3$ samples crystallize in a rhombohedral perovskite phase in the doping range of $0.05 \leq x \leq 0.15$. Moreover, an additional impurity phase corresponding to

$\text{Bi}_{12}\text{NiO}_{19}$ has been spotted around 30° in the 2θ range. Typically, it is very difficult to prepare a single-phase BiFeO_3 , as the product is frequently contaminated with some secondary phases like Bi_2O_3 , $\text{Bi}_2\text{Fe}_4\text{O}_9$ and $\text{Bi}_{12}(\text{Bi}_{0.5}\text{Fe}_{0.5})\text{O}_{19.5}$ [21,25]. The XRD results are in well accord with the reported results by Wang *et al.* [23]

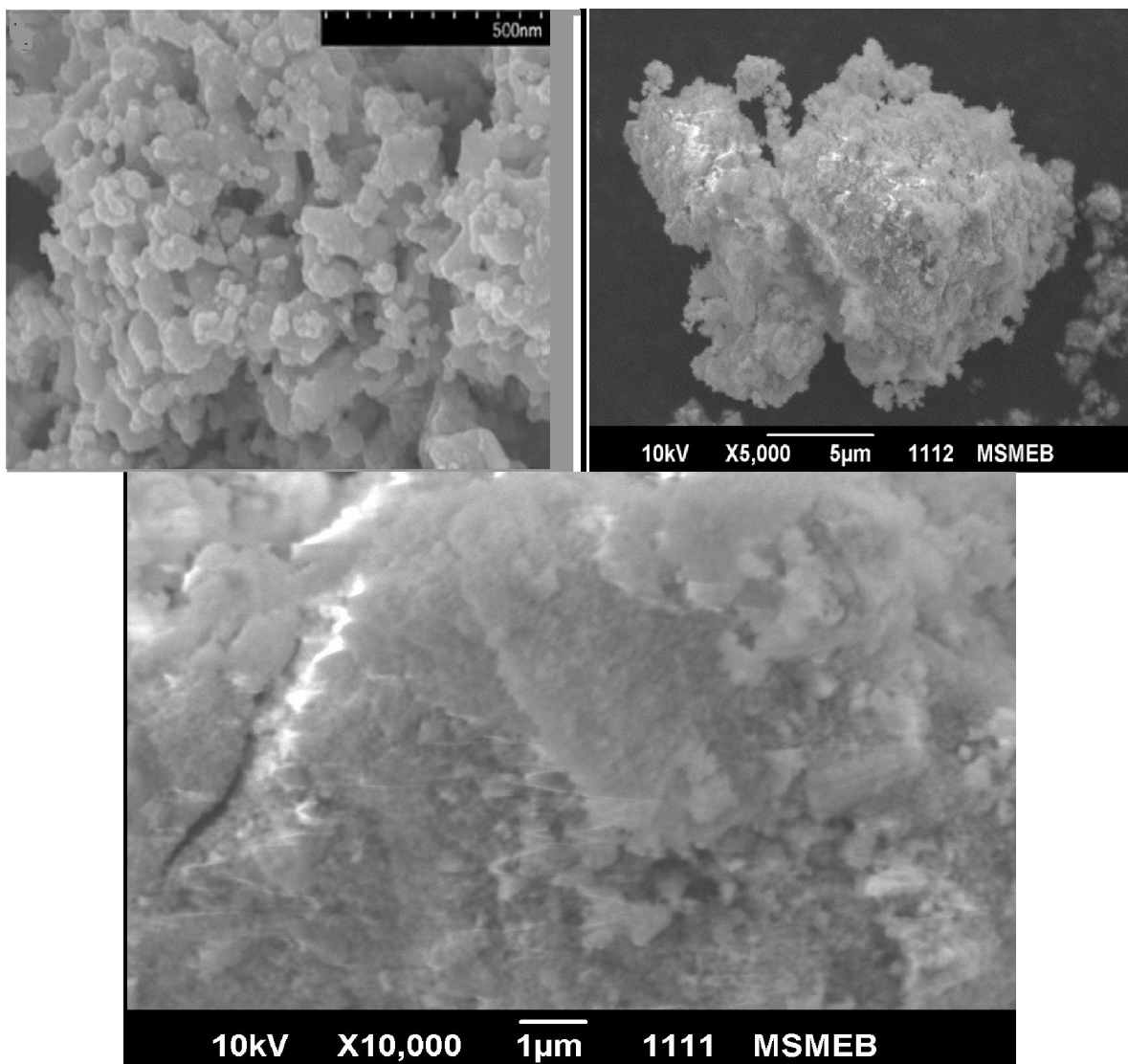


Figure 2.11 SEM Diagram of BFO Doped with Nickel

SEM:

The field emission scanning electron microscope (FESEM) is used to observe the morphological

details of the sample. Figure 3 shows the images of the BFO sample for both undoped and 5mol% Ni-doped after annealing at 500°C in air for 10-12 hr at higher and lower resolutions.

For both pure BFO and Ni-doped sample, anisotropic growth with few interconnected pores

among the agglomerated particulates is noted. Agglomerates have irregular polygonal to bimodal shape structures. Both samples exhibit strong agglomeration tendency among the granular particulates. Particle size for the undoped perovskite bismuth ferrite is about 20 nm while that for Ni-doped sample is found to be about 22 nm.

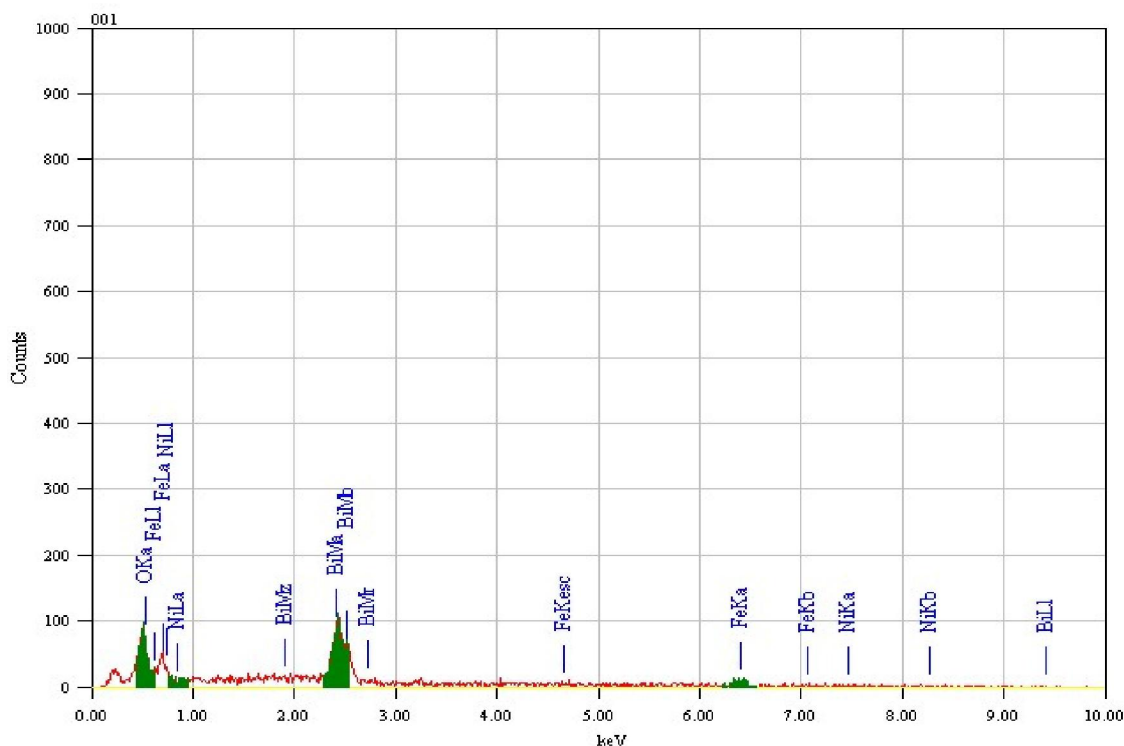


Figure 2.12 EDX Diagram of BFO Doped with Nickel

EDX: The EDX results clearly confirm the presence of essential elements for the successful synthesis of the BFO-based material. Presence of Ni peak exhibits doping effect on the bismuth ferrite matrix which validates with corresponding experimental findings from X-ray diffractogram study with shift in the peak towards left.

Chapter 3

Applications:

There are following applications of BFO and its related compound:

1. Photovoltaics: In the Ferroelectric Photovoltaic effect, a [photocurrent](#) is generated in a ferroelectric material under illumination and its direction is dependent upon the ferroelectric polarization of that material. So, FPV effect has a promising potential as an alternative to conventional photovoltaic devices. But the main hindrance is that a very small photocurrent is generated in ferroelectric materials like LiNbO_3 ^[12], which is due to its large bandgap and low conductivity. In this direction bismuth ferrite has shown a great potential since a large photocurrent effect and above bandgap voltage^[13] is observed in this material under illumination. Most of the works using bismuth ferrite as a photovoltaic material has been reported on its thin film form but in a few reports researchers have formed a bilayer structure with other materials like polymers, [graphene](#) and other semiconductors. In a report *p-i-n heterojunction* has been formed with bismuth ferrite [nanoparticles](#) along with two oxide based carrier transporting layers^[14]. In spite of such efforts the

power conversion efficiency obtained from bismuth ferrite is still very low. [32]

2. Superconductivity: BFO also used as a superconductor by weaken the superconductivity and lower T_c by reducing the number of charge carriers (either electrons or positively-charged holes, depending on the material). One way to lower the carrier concentration is to expose a thin layer of the material to an electric field that repels the carriers, pushing them into the external circuit. But with traditional electrodes, this “field effect” is often too small to change T_c very much.

To produce higher fields, researchers have turned to the large, built-in electric fields that occur in ferroelectric materials. [33]

So for this purpose a team of Javier Villegas of the CNRS/Thales Physics Lab (UMPhy) in Palaiseau, France, and the University of Paris Sud 11 in Orsay, is also decided to try the ferroelectric material bismuth ferrite (BFO). It has an especially large polarization (charge separation), which leads to a large field. They grew BFO on top of a very thin layer of the high-temperature superconductor yttrium barium copper oxide (YBCO) in such a way that the BFO atoms were aligned with the atoms of the superconductor underneath. [35]

3. Spintronics Devices (that includes a spin-based transistor) [29]

4. Information Storage Devices (magnetic tape, floppy disk etc)

5. Spin Valve (device consisting of two or more conducting magnetic materials, that alternate its electrical resistance) [28]

6. Quantum Electromagnets (electromagnets are wire coils or loops, which tend to be bulky and difficult to fabricate)

7. Microelectronic Devices (MOSFETs, Bipolar Transistor etc)

8. Sensors (measures a physical quantity and converts it into a signal which can be read by an instrument)

9. Transducers, Magnetic field sensors and information storage in industry.

10. The data can be written electrically and read magnetically.

11. The best aspect of ferroelectric random access memory (FE RAM) [40]

12. BiFeO₃ potential application of spintronics and photo catalytic compound.....

13. Among all above BiFeO₃ is the only material that is both magnetic and strong ferroelectric. [37]

As a result, it has had an impact on the field of multiferroics that is comparable to that of yttrium barium copper oxide (YBCO) on superconductors, with hundreds of publications devoted to it in the past few years. [30]

14. Nickel nitrate having great magnetic properties if doped with iron and bismuth and also are used in making coins and heat exchange items like valve. The Most of nickel is used to make stainless steel as a protective and ornamental coating for less corrosion. Nickel is combined with many other elements, including chlorine, sulfur, and oxygen. Most of these nickel compounds dissolve easily in water and have a characteristic green or blue color with no characteristic odor or taste. Nickel compounds are used in plating, coloring ceramics, making some batteries, and as chemical reaction catalysts. [28]

Results and discussion:

XRD measurements were performed to characterize the crystal structure of the calcined powders. As shown in Figure 2.9, all the XRD patterns can be indexed to pure rhombohedral perovskite structure. After heat treatment at 550°C, the sample from citric acid precursor begins to generate pure phase BFO while another sample from 350°C is still of amorphous feature. It is clear that the crystallization of BFO completed at a temperature of 550°C for citric acid precursor while 350°C, which is in good line with the analysis. Meanwhile, the particle size of BFO changed remarkably after further heat treatment.

Calcined at temperatures above 450°C, well-crystallized and pure phase BFO can be obtained for either precursor. As discussed in early literatures, the grain sizes of BFO NPs grow up with increasing the temperature in soft chemical routes [21, 26]. This can be also confirmed by the peak sharpening of XRD curves. [41]

The morphology of the calcined BFO nanoparticles was examined by SEM. Typical SEM images are shown in Figure 2.8. It is clear that the spherical NPs formed from both are sufficiently fine and uniform and the particle sizes are about 14nm, respectively.

Our NPs are well crystallized, and both can be indexed to pure BFO rhombohedral crystal structure. The XRD image of individual BFO NP clearly shows an interplanar spacing of 1.39 Å to 4Å. We can expect the size of NPs with an average particle size of about 14 nm through keeping the calcinations temperatures at 450, 550 respectively. Figure 2.8 shows the FTIR spectra of BiFeO₃ precursors using tartaric acid and citric acid as chelating, respectively. As shown, eight characteristic IR peaks appeared for BFO precursor, while four characteristic IR peaks together with some weak peaks appeared for BFO precursor using citric acid as chelating. Both samples have two sharp and one wide IR peaks, which correspond to the stretching vibrations of C=O and –OH. The IR wide peaks located at 3866 cm⁻¹ were assigned to the stretching vibrations of structural hydroxyl (OH) groups, and the intense peaks at 1648–1696 cm⁻¹ were assigned to the stretching vibrations of C=O. The IR peaks located at 1421cm⁻¹ were attributed to the symmetry bending vibration of C–H. In addition, a sharp IR peak located at 1293cm⁻¹ was assigned to the stretching vibration of single bond of C–O for tartaric acid precursor sample, while it cannot be observed for citric acid precursor sample. The IR peaks below 1000 cm⁻¹ (such as 512, 836, and 942cm⁻¹ for tartaric acid precursor, 617, 591, 683, 898, and 990 cm⁻¹ for citric acid precursor) were corresponding to the vibrations bonds of Bi–O or Fe–O, respectively. Firstly, Bi (NO₃)₃·5H₂O and Fe (NO₃)₃·9H₂O along with chelating agents were added to the deionized water and formed the complex of Bi and Fe. Secondly, sol-like precursor and irregular particles come into being followed by aqueous solution were dried. [42]

Phase analysis of Figure of shows the X-ray diffraction of Ni-doped BFO heat treated at 550 °C for 1. Diffraction peak corresponding to maximum intensity 10-12 hr sintering required to seen at particle which matches with the pure phase of bismuth ferrites [17]. The average crystallite size was estimated by Scherrer's formula $t = 0.9 / (\Delta \cos \theta)$ (where t is crystallite size, Δ is half width full maxima, θ is

angle between α_1 and α_2) from XRD data shown in Table 2.1. The crystallite size increases with increasing calcined temperature due to thermally activated diffusion. [39]

Ni-doped BFO powders calcined at 550 °C exhibits a small amount of secondary Bi₂Fe₄O₉ phase, whereas XRD patterns of the samples heat treated at 550 and 600 °C have a few weak peaks of the secondary phase. Thus, in subsequent experiments, annealing temperature was maintained at 500 °C to obtain the desired phase purity. The 3mol% Ni-doped BFO annealed at 550 °C shows very weak peaks of the secondary Bi₂Fe₄O₉ phase. When concentration of dopant increases to the extent of 5 and 10mol%, peaks of Bi₂Fe₄O₉ phase remain similar which are shown in Fig. 2.1. However, the crystallite size for the sample with 5mol% doping is found to be smaller than 3 and 10mol% doping. The crystallite sizes of all samples are given in Table 1. The secondary phase does not induce any constraints to the properties of nanocrystallite BFO as it can be seen from the subsequent observations. It was also shown that it is difficult to remove the secondary phase even by strong concentrated nitric acid leaching.

Figure 2.10 shows the small shifting of the strongest XRD peak due to the doping of BFO with Ni. The crystallite size of 5mol% Ni doped bismuth ferrite is about 15.4 nm compared to the undoped perovskite bismuth ferrite which is about 14.7 nm. Atomic radius of Ni²⁺ (0.72Å) is comparable with Fe³⁺ (0.64Å) which may be the possible reason for doping of B site of ABO₃ perovskite (bismuth ferrite) with transitional metal ion. Due to the slight variation atomic radius, strain will be generated in the matrix which may be the cause for slight reduction of crystallite size in Ni-doped sample 3.2. Microstructural and elemental analysis The synthesized powder is spread over a conducting carbon tape, and a field emission scanning electron microscope (FESEM) is used to observe the morphological details of the sample. Figure 3 shows the images of the BFO sample for both undoped and 5mol% Ni-doped after annealing at 500 °C in air for 30 minutes at higher and lower resolutions. For both undoped and Ni-doped sample, anisotropic growth with few interconnected pores among the agglomerated particulates is noted. Agglomerates have irregular polygonal to bimodal shape structures. Both samples exhibit strong agglomeration tendency among the granular particulates. Particle size for the undoped perovskite bismuth ferrite is about 20 nm while that for Ni-doped sample is found to be about 22 nm. The above results are closely connected to the experimental findings from our crystallite size measurement from XRD studies using Scherrer's formula. Hence, we confirmed that synthesis of the

nanocrystalline undoped and Ni-doped bismuth ferrite with perovskite structure was performed successfully.

Conclusions:

Chemical route can be used to synthesize nanocrystalline undoped and Ni-doped bismuth ferrite with perovskite structure and crystallite size of about 14nm and 15.4 nm, respectively. Rise in doping concentration leads to generation of secondary phase, thus dopant concentration is maintained to 5mol%. Morphological analyses exhibits irregular polygonal to bimodal shape agglomerates with few interconnected pores. Dielectric constant for the undoped bismuth ferrite is about 100, while for 5mol% Ni doped sample it is noted around 600 (at low frequency). Such drastic change leads to higher polarizability which also enhances ferroelectricity with Ni doping on perovskite bismuth ferrite. Both nanocrystalline and Ni-doped BFO exhibits super paramagnetic nature due to suppression of spin cycloid magnetic moment. Saturation magnetization of Ni-doped is slightly lower than for undoped BFO due to smaller crystallite size.

References:

1. Drexler, K. Eric (1986). Engines of Creation: The Coming Era of Nanotechnology. Doubleday. ISBN 0-385-19973-2. Jump up ^ Apply nanotech to up industrial, agri output, *The Daily Star* (Bangladesh), 17 April 2012.
2. Chaudhari YA, Singh A, Abuassaj EM, *et al.* Multiferroic properties in BiFe_{1-x}Zn_xO₃ (x = 0.1–0.2) ceramics by solution combustion method (SCM).
3. Qin W, Guo YP, Guo B, *et al.* Dielectric and optical properties of BiFeO₃–(Na_{0.5}Bi_{0.5}) TiO₃ thin films deposited on Si substrate using LaNiO₃ as buffer layer for photovoltaic devices. *J Alloys Compd* 2012.
4. S. Li, Y.-H. Lin, B.-P. Zhang, C.-W. Nan, and Y. Wang, "Photocatalytic and magnetic behaviors observed in nanostructured BiFeO₃ particles," *Journal of Applied Physics*, vol. 105, no. 5, Article ID 056105, 2009.
5. T.-J. Park, G. C. Papaefthymiou, A. J. Viescas, A. R. Mooden baugh, and S. S. Wong, "Size-dependent magnetic properties of single-crystalline multiferroic BiFeO₃ nanoparticles," W. Eerenstein, N. D. Mathur, and J. F. Scott, "Multiferroic and magnetoelectric materials," *Nature*, vol. 442, no. 7104, pp.759–765, 2006.
6. P. Fischer, M. Polomska, I. Sosnowska, and M. Szymanski, "Temperature dependence of the crystal and magnetic structures of BiFeO₃," *Journal of Physics C*, vol. 13, no. 10, pp. 1931–1940, 1980.
7. C. Tabares-Munoz, J. P. Rivera, A. Monnier, and H. Schmid, "Measurement of the quadratic magnetoelectric effect on single crystalline

- BiFeO₃,” *Japanese Journal of Applied Physics*, vol. 24, pp. 1051–1053, 1985.
8. Y. P. Wang, L. Zhou, M. F. Zhang, X. Y. Chen, J.-M. Liu, and Z. G. Liu, “Room-temperature saturated ferroelectric polarization in BiFeO₃ ceramics synthesized by rapid liquid phase sintering,” *Applied Physics Letters*, vol. 84, no. 10, pp. 1731–1733, 2004.
 9. M. Fiebig, T. H. Lottermoser, D. Fröhlich, A. V. Goltsev, and R. V. Pisarev, “Observation of coupled magnetic and electric.
 10. I. E. Dzyaloshinskii, *Sov. Phys. JETP* 10, 628 (1960).
 11. D. N. Astrov, *Sov. Phys. JETP* 11, 708(1960).
 12. V. J. Folen et al., *Phys. Rev. Lett.* 6, 607(1961).
 13. Hans Schmid, *Ferroelectrics* 162, 317-338 (1994).
 14. Daniel Khomskii *Physics* 2, 20 (2009).
 15. A. M. Glazer, *Acta Cryst.* B28, 3384 (1972).
 16. J. A. Bartkowska, *International Journal of Thermophysics* 32, 739 (2011).
 17. Smolensky GA, Isupov VA, Agronovskaya AI, *Sov Phys Solid State* 1, 150 (1959).
 18. Achenbach GD, James WJ, Gerson R, *Am J. Ceram Soc.* 50, 437 (1967).
 19. Kubel F, Schmid H. *Acta Crystallogr B* 46, 698 (1990).
 20. Spaldin, K. M. Rabe, M. Wuttig and R. Ramesh, *Science* 299, 1719 (2003).
 21. A. K. Zvezdin, and D. Viehland, *Appl. Phys. Lett.* 84, 5261_ (2004).
 22. C. Ederer and N. A. Spaldin, *Phys. Rev. B* 71, 224103 (2005).
 23. Ederer C, Spaldin NA. *Phys Rev. B* 71, 224103 (2005).
 24. Mei Z. G, Shang S, Wang Y, Liu Z-K. *Apply Phys. Lett.* 98, 131904 (2011).
 25. G. Catalan and J. F. Scott, *Advanced Materials*, 21, 2463 (2009).
 26. A. G. Gavriliuk et al., Phase transition with suppression of magnetism in BiFeO₃ at high pressure. *Condensed Matter* 4, Volume 82, 224 (2005).
 27. a) Palemiec A. et al., *Act Cryst. B* 63: 537 (2007).
 28. b) Palemiec A. et al., *Acta Phys. Pol. A* 117, 296 (2010).
 29. Scott JF. *J Magn Magn. D. J. Norris*, (1995). "Measurement and Assignment of the Size-Dependent Optical Spectrum in Cadmium Selenide (CdSe) Quantum Dots, MIT". *hdl:1721.1/11129 (1995)*.
 30. "Nanotechnology Information Center: Properties, Applications, Research, and Safety Guidelines". American Elements (1998).
 31. M. Cahay (2001). *Quantum Confinement VI: Nanostructured Materials and Devices: Proceedings of the International Symposium*. The Electrochemical Society. ISBN 978-1-56677-352-2. Retrieved 19 June 2012.
 32. H. Haug; Stephan W. Koch (1994). *Quantum Theory of the Optical and Electronic Properties of Semiconductors*. World Scientific. ISBN 978-981-02-2002-0. Retrieved 19 June 2012.
 33. T. V. Lippen, R. No'izel, G. J. Hamhuis, and J. H. Wolter, *J. Appl. Phys.* 97, 044301 (2005).
 34. R. G. Nuzzo and D. L. Allara, *J. Am. Chem. Soc.* 105, 4481 (1983).
 35. M. Giersig and P. Mulvaney, *Langmuir* 9, 3408(1993).
 36. S. Chaure, N. B. Chaure, and R. K. Pandey, *J. Nanosci. Nanotechnol.* 7, 945(2007).
 37. J. Mazher, S. Badwe, R. Sengar, D. Gupta, and R. K. Pandey. *Physica E* 16, 209 (2003).
 38. S. Chaure, N. B. Chaure, and R. K. Pandey, *J. Nanosci. Nanotechnol. Journal of Applied physics* 98(4).
 39. P. M. Aneesh et al. (2007) “ synthesis of ZnO nanoparticles by hydrothermal method” nanophotonic material IV, *Proc. Of SPIE Vol.* 6639, 66390J.
 40. S Ilcan, Caglar Y., Caglar M., (2008), Preparation and characterization of ZnO thin films deposited by sol-gel spin coating method. *Journal of optoelectronics and advanced materials.* 10:2578–2583.
 41. L. E. Brus. Electron-electron and Electron – hole interaction in small semiconductor crystallites: The size dependence of the lowest excited electronic state. *Journal of Chemistry Physics.* 80. 9. 1984.
 42. Y. Wang, A. Suna, W. Mahler, and R. Kasowski, *J. Chem. Phys.* 87, 7315 (1987).
 43. L.W. Wang and A. Zunger, *Phys. Rev. B.* 51, 17398(1995).
 44. P. E. Lippens and M. Lannoo, *Phys. Rev. B.* 39, 10935(1989).
 45. L. E. Brus, *J. Chem. Phys.* 80, 4403(1984).
 46. N. A. Hill and K. B. Whaley, *J. Chem. Phys.* 100, 2831(1994).
 47. S. Sapiro and D. D. Sharma, *Phys. Rev. B.* 69, 125304(2004).
 48. H. Fu and A. Zunger, *Phys. Rev. B.* 55, 1642(1997).